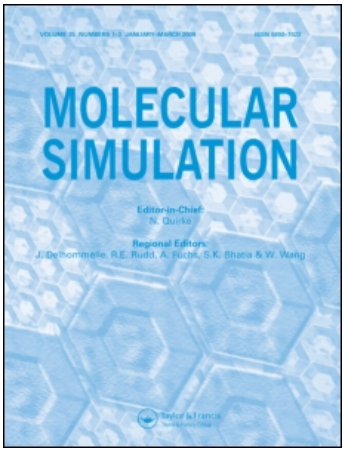

Molecular Simulation
Publication details, including instructions for authors and subscription information:
http://www.informaworld.com/smpp/title~content=t713644482

A first-principles study of H_2O adsorption and dissociation on the $SrTiO_3(100)$ surface

Beverly Brooks Hinojosa[a]; Tim Van Cleve[a]; Aravind Asthagiri[a]
[a] Department of Chemical Engineering, University of Florida, Gainesville, FL, USA

Online publication date: 03 August 2010

To cite this Article Hinojosa, Beverly Brooks , Van Cleve, Tim and Asthagiri, Aravind(2010) 'A first-principles study of H_2O adsorption and dissociation on the $SrTiO_3(100)$ surface', Molecular Simulation, 36: 7, 604 — 617
To link to this Article: DOI: 10.1080/08927021003762746
URL: http://dx.doi.org/10.1080/08927021003762746

Molecular Simulation
Vol. 36, Nos. 7–8, June–July 2010, 604–617

Taylor & Francis
Taylor & Francis Group

A first-principles study of H_2O adsorption and dissociation on the $SrTiO_3(100)$ surface

Beverly Brooks Hinojosa, Tim Van Cleve and Aravind Asthagiri*

Department of Chemical Engineering, University of Florida, Gainesville, FL 32611, USA

(*Received 19 January 2010; final version received 9 March 2010*)

We use density functional theory (DFT) to examine the adsorption of H_2O on the SrO- and TiO_2-terminated $SrTiO_3(100)$ surface. At coverages of 0.5 monolayer (ML), we find that water preferentially binds associatively on the TiO_2 termination by 0.2 eV/H_2O and negligible differences in energy between associated and dissociated H_2O on the SrO termination. These results are in agreement with an earlier hybrid Hartree–Fock-DFT study and the general conclusions from several experimental studies. But at coverages below 3/8 ML, our DFT calculations predict a crossover to preference for dissociative H_2O on the TiO_2 termination. On the SrO termination, the use of larger surface supercells (2×2) allows for the stabilisation of mixed adsorption configuration at 1/2 ML and subsequent decrease in coverage results in dissociative water configurations. We explored dimer configurations of molecular H_2O and HO—H_2O complexes at 1/4 ML coverage but these configurations are less stable than the isolated dissociated state. The energy barrier for dissociation of H_2O on the TiO_2 termination at 1/8 ML coverage is found to be 0.08 eV, which suggests that the dissociated state is both favoured energetically and kinetically at low coverages and temperatures. These low coverage results from our DFT study conflict with existing experimental studies and we present scenarios that can be explored both experimentally and theoretically to resolve this discrepancy.

Keywords: density functional theory; oxide surfaces; water; $SrTiO_3$

1. Introduction

The adsorption and reactivity of water on low-Miller index oxide surfaces serves as a model system to understand the structure–reactivity relationship of oxide surfaces. Water–oxide interfaces are also important in a range of applications in catalysis, environmental remediation and biomineralisation. Even under ultrahigh vacuum (UHV) conditions, it is often difficult to avoid contamination of low coverages of water, which can affect the reactive properties of the surface. An important first step in understanding the reactive behaviour of H_2O–oxide interfaces is to resolve whether water adsorbs associatively or dissociatively on the oxide surface. While one may expect that the characterisation of the structure of water on low-Miller index oxide surfaces under UHV conditions should be readily resolved with a combination of experimental and theoretical studies, the literature, for example on H_2O on rutile $TiO_2(110)$ [1–3] and MgO(100) [1,4–6], shows that conflicting models can exist and are non-trivial to resolve. This challenge in resolving the structure of water on the oxide is due in part to a combination of the difficulty of controlling oxide surface reconstructions, contaminants in UHV, coverage effects, the potential presence of complex water clusters and approximations that must often be made in first-principles studies (e.g. size of system, accuracy of exchange-correlation functionals).

Water adsorption on $SrTiO_3(100)$, including the role of defects such as oxygen vacancies and step edges, has been the focus of several experimental studies [7–13]. Like many oxides, $SrTiO_3$ can have multiple terminations for a given surface plane and $SrTiO_3(100)$ can be terminated by a SrO or a TiO_2 plane (see illustration in Figure 1). The presence of the TiO_2 termination of $SrTiO_3(100)$ has motivated some of the studies of H_2O on this surface, since it offers an opportunity to compare with the extensive studies of TiO_2 surfaces to shed light on the role of structure on the chemistry of the oxide [7]. $SrTiO_3$ also garners interest for potential use as a catalyst in photoelectric splitting of water [14,15].

Ultraviolet and X-ray photoemission spectroscopy (UPS and XPS) studies of water on $SrTiO_3(100)$ under UHV conditions suggest that water adsorbs molecularly on the pristine surface, but upon the inducement of oxygen vacancies via ion bombardment [10–13] or step edges by vacuum fracturing [8,9], the presence of dissociated water is detected. High resolution electron energy loss spectroscopy (HREELS) has also been used to probe the phonon modes of H_2O and D_2O on stoichiometric and reduced $SrTiO_3(100)$ [10–12]. While the identification of phonons attributed to the adsorbate is complicated by the overlap with surface phonons of the oxide, the HREELS study suggests that water adsorbs dissociatively on $SrTiO_3(100)$ only in the presence of oxygen vacancies [10,11]. Lopez et al. [16] reported in another HREELS

*Corresponding author. Email: aasthagiri@che.ufl.edu

ISSN 0892-7022 print/ISSN 1029-0435 online

DOI: 10.1080/08927021003762746
http://www.informaworld.com

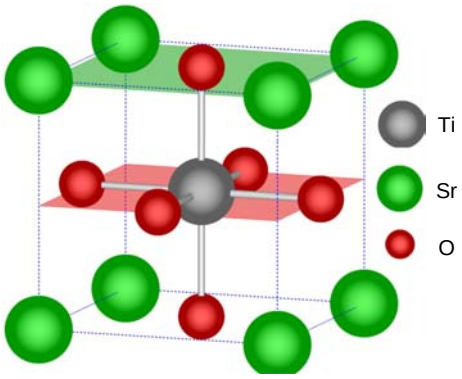

Figure 1. The bulk unit cell of $SrTiO_3$ highlighting the SrO termination (top) and TiO_2 termination (middle) of the $SrTiO_3(100)$ surface.

study that the presence of Na on the $SrTiO_3(100)$ surface can also result in dissociative adsorption of water. Wang et al. [7] have performed to date the only temperature programmed desorption (TPD) experiments in UHV of water adsorption on $SrTiO_3(100)$. They found that water adsorbs on the pristine $SrTiO_3(100)$ with a maximum peak desorption temperature of 260 K, which shifts to lower temperatures with increasing water coverage. The TPD study also concludes non-dissociative adsorption on the $SrTiO_3(100)$ surface with the primary evidence that the observed peak temperature in the TPD is too low to be assigned to dissociated H_2O. They approximated the surface to consist of $\sim$80% TiO_2 termination and have confirmed via low energy electron diffraction (LEED) that the bare surface is initially the (1×1) unreconstructed $SrTiO_3(100)$ surface. After sputtering the surface, the TPD spectra show a long tail starting at $\sim$300 K and decaying at around 480 K. This tail in the TPD spectra is assigned to dissociated water on O vacancies and matches the general conclusions from earlier XPS and UPS studies of reduced $SrTiO_3(100)$ surfaces. Wang et al. [7] suggested that the lack of bridging O atoms on the pristine TiO_2-terminated $SrTiO_3(100)$ surface prevents strong H-bonding with the surface O atoms that would make it favourable to strip the H atoms from the water molecule. In comparison, water binds dissociatively (associatively) on the defect-free $TiO_2(100)$ ($TiO_2(110)$) surfaces [17–19]. Density functional theory (DFT) calculations suggest that on $TiO_2(100)$, the adsorbed water molecule has access to low-coordinated bridging O atoms, but on $TiO_2(110)$ the distance between the H-atoms on the water molecule and the bridging O atoms is longer and prevents strong formation of H-bonds with the oxide surface O atoms [7,20]. In summary, the experimental results to date point to a model of associative adsorption of H_2O on pristine $SrTiO_3(100)$ surface, with dissociation only observed at defects such as O vacancies and step edges.

In this paper, we report on DFT calculations of H_2O adsorption and dissociation on both terminations of $SrTiO_3(100)$. There has been a recent hybrid Hartree–Fock (HF)-DFT study examining water on both terminations of $SrTiO_3(100)$ and found that molecular water is favoured over dissociated water on both terminations with this difference more pronounced on the TiO_2 termination [21]. This earlier DFT study examined coverages down to 1/2 monolayer (ML) on a 1×1 surface cell (see Section 2 for definition of 1 ML for this system). We have explored more dilute coverages down to 1/8 ML using a 2×2 surface cell and find that both the adsorption energy and structure of water are sensitive to coverage. At coverages below 1/2 ML, DFT predicts that dissociated H_2O is favoured on both terminations of $SrTiO_3(100)$. We discuss possible sources of the differences between our DFT results and the existing experimental studies.

2. Calculation details

All the DFT calculations in this paper were performed with the Vienna *ab initio* simulation package (VASP) [22–25] using the projector augmented wave [26,27] pseudopotentials provided in the VASP database. We included the Sr (4s, 4p, 5s), Ti (3s, 3p, 3d, 4s) and O (2s, 2p) orbitals as valence states and used a plane wave cut-off energy of 400 eV. Calculations have been done using the generalised gradient approximation Perdew–Burke–Ernzerhof (GGA-PBE) exchange correlation functional [28]. We will discuss the effects of the functional on the accuracy of the DFT calculations in Section 3.4.1. Electronic relaxation was performed with a block Davidson iteration method accelerated using Fermi-level smearing with a Gaussian width of 0.1 eV [29]. All calculations used a 6-layer slab with the bottom two layers fixed. The system is relaxed until all the forces are less than 0.03 eV/Å. We tested 8-layer and 10-layer slabs to confirm the binding energy and adsorbate structure match that were found on the 6-layer slab. The water adsorbates were examined in increments of 1/2 and 1/8 ML for the 1×1 or 2×2 surface unit cells, respectively. We define 1 ML as 2 water molecules per surface cation, which matches the definition used by the earlier HF-DFT study [21]. A vacuum region of about 24 Å is included to prevent the slab from interacting with its periodic image in the surface normal direction. We completed all calculations using dipole corrections in the surface normal direction [30]. The effects of spin polarisation corrections were checked and found not to affect the adsorption energy for any of the high symmetry sites. We use an $8 \times 8 \times 1$ and $4 \times 4 \times 1$ Monkhorst–Pack mesh [31] for the 1×1 and 2×2 surface unit cells, respectively. We found a bulk lattice constant of 3.95 Å for $SrTiO_3$, which matches fairly well with that previously reported from experiment (3.90 Å) [32] and DFT (3.94 Å) [33]. Minimum energy

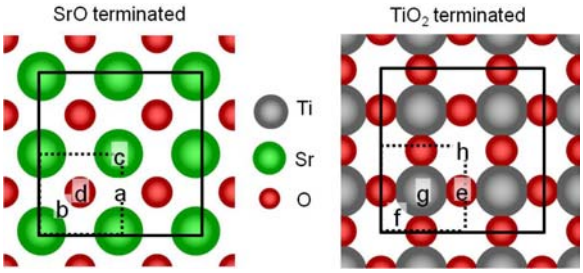

Figure 2. The top layer of the (a–d) SrO-terminated and (e–h) TiO_2-terminated $SrTiO_3(100)$ surface showing the 1×1 (2×2) surface cell outlined by dashed (solid) lines. The high symmetry adsorption sites we examined are identified on the SrO termination as (a) fourfold, (b) bridge, (c) Sr, (d) O and on the TiO_2 termination as (e) O, (f) bridge, (g) Ti and (h) fourfold.

pathways and the barrier to water dissociation are calculated using the nudged elastic band (NEB) method [34–36].

3. Results and discussion

3.1 Half-monolayer H_2O on $SrTiO_3(100)$

On the (1×1)-$SrTiO_3(100)$ surface, we examined four high symmetry adsorption sites for both the SrO- and TiO_2-terminated surfaces, with each shown in Figure 2. Figure 2(a)–(d) highlights the fourfold hollow site, the bridge site between the surface O and Sr, on top the Sr and O atoms, respectively, for the SrO-terminated surface. Figure 2(e)–(h) illustrates the surface sites for on top O, the bridge site between surface Ti and O, on top surface Ti and the fourfold hollow site, respectively, for the TiO_2-terminated surface. For simplicity, we will refer to these sites as fourfold, bridge, Sr, Ti and O. The adsorption of one water molecule on a single high symmetry site for this surface unit cell corresponds to a surface coverage of 1/2 ML, with ML defined in Section 2. We initially placed molecular water with the oxygen atom in each of the high symmetry surface sites with various orientations for the hydrogen atoms ranging from pointing away from, perpendicular to and downward towards the surface atoms. After relaxation, the final adsorbate configurations depend only on the surface adsorption site (i.e. the initial oxygen position) and not on the initial hydrogen orientation.

Table 1 reports the adsorption energy for each of the surface adsorption sites at both 1/2 and 1/8 ML coverages. The adsorption energy (E_{ads}) is defined as:

$$E_{ads} = \frac{\left\{\left(E_{slab} + N \times E_{H_2O,gas}\right) - E_{H_2O,slab}\right\}}{N}, \quad (1)$$

where E_{slab} is the total energy of the relaxed $SrTiO_3$ slab in the absence of any adsorbed H_2O, $E_{H_2O,gas}$ is the energy of an isolated water molecule, $E_{H_2O,slab}$ is the total energy of the $H_2O/SrTiO_3$ slab and N is the total number of water molecules in the $H_2O/SrTiO_3$ slab. Figure 3(a)–(d) illustrates the most favoured associative and dissociative H_2O configuration on the SrO and TiO_2 terminations of $SrTiO_3(100)$ at 1/2 ML. Table 2 presents all the relevant bond lengths associated with the structures illustrated in Figure 3(a)–(d), along with similar values at the 1/8 ML configuration. We focus on the results at 1/2 ML in this section and return to low coverage results in Section 3.2. To distinguish between hydroxyl groups consisting of O atom coming from the water vs. the oxide surface, the O atom from water (oxide surface) will be denoted by O_w (O_x).

The most favoured state for molecular H_2O is the bridge site for both terminations. On the SrO termination, the bridge site is more stable by 0.26 eV over the fourfold site and similarly on the TiO_2 termination the bridge site is favoured over water adsorption on the Ti atom by 0.18 eV. A previous investigation using hybrid HF-DFT with a linear combinations of atomic orbital calculations studied water on $SrTiO_3(100)$ and found both stable molecular and dissociative states on both terminations [21]. To test the favourability of dissociative binding, we separated one hydrogen from the converged molecular $H_2O/SrTiO_3(100)$ and placed it near the neighbouring surface oxygen. On both terminations, we found after minimisation that the dissociated H atom recombines with the hydroxyl group to form molecular water. Evarestov et al. [21] also reported difficulties stabilising a dissociative state at 1/2 ML

Table 1. Adsorption energy (E_{ads}) of water at 1/8 and 1/2 ML on various high symmetry sites, defined in Figure 2, on the SrO- and TiO_2-terminated $SrTiO_3(100)$.

	E_{ads} (eV/H_2O)			
	SrO termination		TiO_2 termination	
Adsorption site	1/8 ML on 2×2	1/2 ML on 1×1	1/8 ML on 2×2	1/2 ML on 1×1
Fourfold	0.90 (1.31)	0.58 (0.85)	0.23	0.05
Bridge	Unstable (1.14)	0.84 (Unstable)	0.89 (1.11)	0.79 (0.59)
Sr/Ti	Converges to fourfold	Converges to fourfold	0.76	0.61
O	0.11	0.06	0.72	Converges to top Ti

Note: The values in parentheses correspond to a dissociative state.

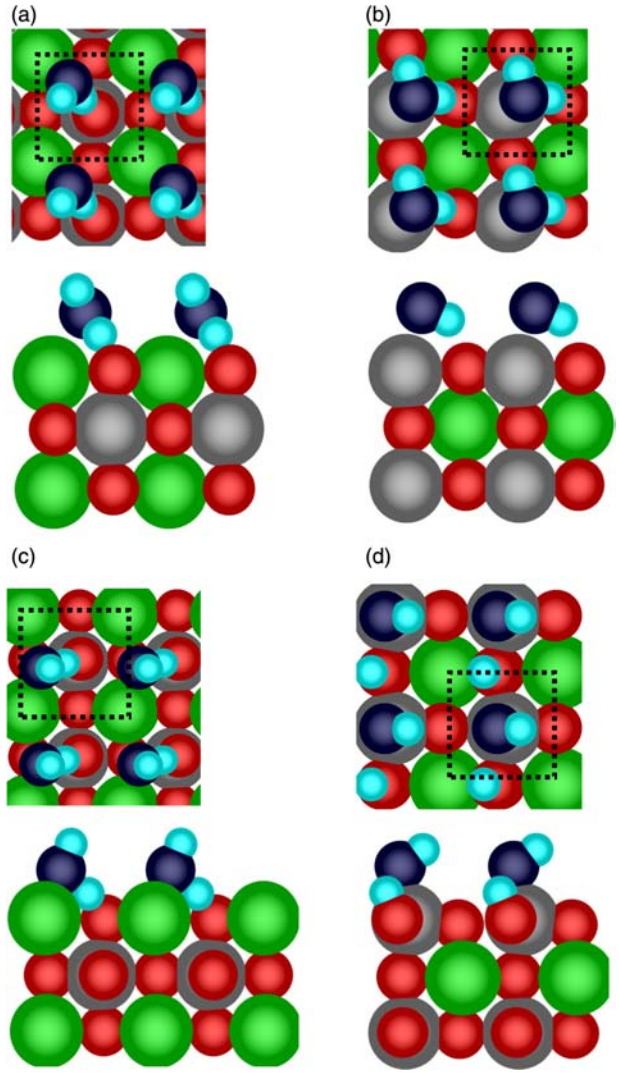

Figure 3. Most favoured half monolayer molecular (a,b) and dissociative (c,d) water configuration on 1×1-SrO (a,c) and 1×1-TiO_2 (b,d) termination as viewed along the [001] direction (above) and the [100] direction (below). The 1×1 surface unit cell is outlined by the dashed box.

coverage on the 1×1 surface cell of $SrTiO_3(100)$ [21]. To overcome these difficulties, they used the stabilised dissociated water on $SrZrO_3(100)$ surfaces and scaled the resulting configuration to the $SrTiO_3(100)$ surface. Upon relaxation of this structure, they were able to obtain a stable dissociated configuration on the $SrTiO_3(100)$ surfaces. We were able to finally stabilise a dissociative state using an initial configuration based on the structure reported by Evarestov et al. [21]. The primary feature of the dissociated structure of Evarestov et al. is the distance between the hydroxyl group and the surface cation. If this distance is appropriate in the initial dissociated structure, a local minimum of the dissociative H_2O can be stabilised on both terminations. However, the dissociative state on TiO_2 is found to be less stable by 0.2 eV/H_2O and there is a negligible difference between associative and dissociative H_2O (0.01 eV/H_2O) on the SrO termination (see Table 1). Our values for the relative stability of associative vs. dissociative H_2O on both terminations are very similar to the earlier HF-DFT study where it was reported that molecular H_2O is favoured by 0.1 eV/H_2O on the TiO_2 termination and 0.003 eV/H_2O difference on the SrO termination [21]. As can be seen in Figure 3(c), water rotates out of the bridge site and into a fourfold site on SrO, following dissociation. The values for the bond lengths of the minima structures determined in our study also agree well with those reported by Evarestov et al. with slight underestimation of the O_w—Sr at 2.55 Å vs. 2.61 Å [21] and overestimation of the O_w—Ti at 1.90 Å vs. 1.88 Å [21].

The primary conclusion from the earlier DFT study, and our values at 1/2 ML, is that H_2O should be expected to adsorb associatively on the defect-free $SrTiO_3(100)$ surface. This conclusion agrees with the general findings of various experimental studies [7–13], especially if the expectation of predominance of TiO_2 termination in these experiments is taken into consideration [7]. While adsorption energies were not extracted in the TPD study of H_2O adsorption on $SrTiO_3(100)$ [7], we can

Table 2. Bond lengths for the most stable water adsorbate configurations at 1/8 and 1/2 ML coverage on the SrO- and TiO_2-terminated $SrTiO_3(100)$ surface.

	SrO termination				TiO_2 termination			
	1/8 ML (2×2)		1/2 ML (1×1)		1/8 ML (2×2)		1/2 ML (1×1)	
Bond length	H_2O	H—OH	H_2O	H—OH	H_2O	H—OH	H_2O	H—OH
O_w—H_1	1.03	0.97	0.97	0.97	0.98	0.97	0.98	0.97
O_w—H_2	1.03	1.59	1.07	1.30	1.00	2.84	1.00	2.23
(Sr,Ti)—O_w	2.71	2.59	2.58	2.55	2.21	1.84	2.27	1.90
O_x—H_1	1.62	3.39	3.04	2.97	2.18	2.77	2.42	2.91
O_x—H_2	1.62	1.01	1.45	1.13	1.88	0.98	1.82	0.99

Note: Molecular and dissociative states are noted as H_2O and H—OH, respectively.

approximate these values from the peak temperature (T_p) associated with dilute coverages ($\sim$260 K) and assuming first-order desorption with no adsorbate interaction and a prefactor (ν_o) of 1×10^{13}. With these assumptions and a heating rate of 1 K/s [7], a value for the adsorption energy of 0.92 eV can be extracted for $T_p = 260$ K. This adsorption energy is larger than the DFT value of 0.79 and 0.84 eV on the TiO_2 and SrO termination, respectively, which is not unexpected since the 260 K peak temperature is associated with dilute coverages but suggests that the adsorption energies from DFT are qualitatively similar to that derived from experiment. Ignoring the adsorbate–adsorbate interactions, a value of 0.63 eV for the adsorption energy ($T_p \sim 180$ K) at high coverages can be obtained from the TPD spectra. While these values are not very accurate due to the assumptions, they do illustrate a strong coverage dependence on the adsorption energy that can also be observed from the strong shift in the TPD spectra with coverage [7].

3.2 *Dilute coverage of H_2O on $SrTiO_3$(100)*

To probe coverage effects on the adsorption energy and structure of water on the $SrTiO_3$(100) surface, we used a 2×2 surface unit cell, which reduces the possible coverage increment to 1/8 ML. We examined water in the same adsorption sites as above and the E_{ads} for each site is summarised in Table 1 and Figure 4 shows the most stable minima for associative and dissociative H_2O found on both terminations at 1/8 ML. For both terminations, there is a general increase in adsorption energy for both the dissociated and molecular water states, but more importantly a crossover to a preference for the dissociative state occurs when the coverage is decreased from 1/2 to 1/8 ML. For the SrO termination, we observe a stable dissociated state at the fourfold site with an adsorption energy of 1.31 eV/H_2O and is shown in Figure 4(c). As discussed in Section 3.1, dissociated water on the bridge site could not be stabilised in the 1×1 surface cell, and the dissociative state could only be stabilised by shifting to a fourfold site (see Figure 3(c)). The lower coverage further stabilises the dissociative state as evident by the more substantial separation of the O_w—H and free H as seen in Figure 4(c) vs. Figure 3(c). At a coverage of 1/8 ML, the bridge site does have a stable state associated with dissociated water (not shown), but this site is less favourable over the fourfold by 0.17 eV/H_2O. For molecular H_2O, the effect of lower coverage acts in an inverse way and destabilises the water molecule at the bridge site. At 1/2 ML on the 1×1-SrO termination, the molecular water is prevented from dissociating due to repulsive neighbour interactions with an adjacent hydroxyl group in the [100] direction due to periodic boundary conditions, but at lower coverages, this obstacle is removed and the water molecule dissociates as it would prefer in the absence of this repulsive interaction. The most stable molecular water state at 1/8 ML is then found on the fourfold site (see Figure 4(a)), and while this state gains 0.32 eV in stability due to the decrease in coverage, the adsorption energy of 0.90 eV/H_2O is weaker by 0.41 eV/H_2O than the dissociated state. Therefore, our DFT results suggest that at lower coverages dissociated water should be favoured on the SrO termination.

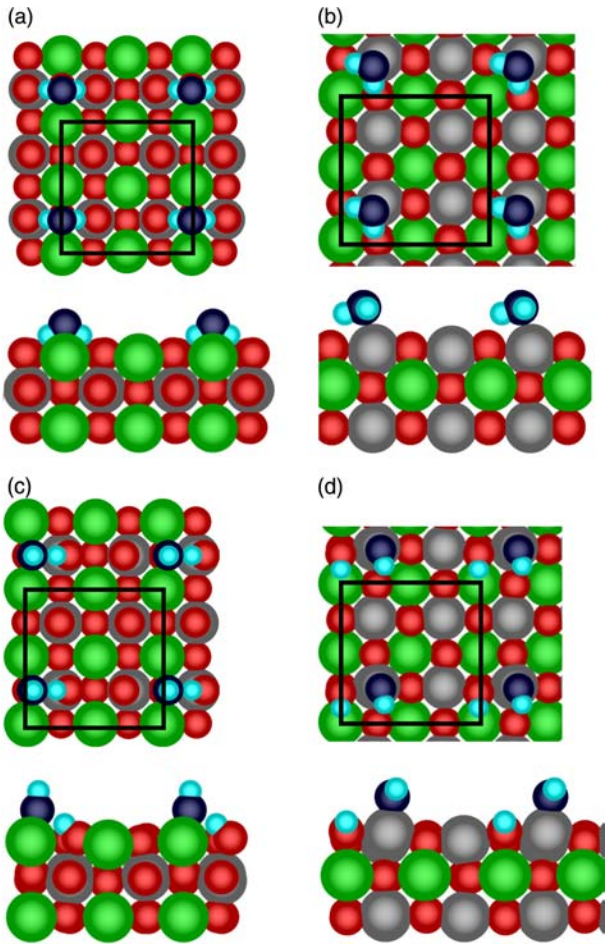

Figure 4. Most favoured 1/8 monolayer molecular (a,b) and dissociative (c,d) water configuration on 2×2 SrO (a,c) and 2×2 TiO_2 (b,d) terminations as viewed along the [001] direction (above) and the [100] direction (below). The 2×2 surface unit cell is outlined by the solid box for visual aid of the top view along the [001] direction.

On the TiO_2 termination of the 2×2 surface cell, we find an increase in molecular water stability at each site with respect to the 1/2 ML coverage on the 1×1 TiO_2-terminated surface. The dissociated water structure at the bridge site on the TiO_2 termination shown in Figure 4(d) has an adsorption energy of 1.11 eV/H_2O, which is 0.22 eV/H_2O more stable than the most stable molecularly bound water shown in Figure 4(b). Therefore, similar to the

SrO termination, there is a crossover to the dissociated state at lower coverages on the TiO_2 termination. Evarestov et al. described the dissociated water configuration on the 1×1-TiO_2 termination as having two hydroxyl groups in a *trans*-position to each other (see Figure 3(d)). On the 2×2-TiO_2 termination, we identified a *cis*-type configuration of the two hydroxyl groups, as illustrated in Figure 4(d). We tested the stability of a *trans*-type configuration of the two hydroxyl groups at the coverage of 1/8 ML and found a nearly energy equivalent state with an E_{ads} of 1.13 eV/H_2O.

The structural information for the most stable water configurations at 1/8 ML is reported in Table 2 and can be compared with the values at 1/2 ML. As noted above for the SrO termination, there is a shift in the site of the preferred molecular water, therefore some of the changes in the structural parameters are due to this change. For dissociated H_2O on the SrO termination, the primary change is a decrease in the O_x—H distance from 1.13 to 1.01 Å when the coverage decreases to 1/8 ML. The distance of 1.01 Å is very close to the value of the hydroxyl group from the water molecule (0.97 Å), which implies that the hydroxyl group associated with O_x increases in strength upon the decrease in coverage. On the TiO_2 termination, there are less dramatic changes in the structure of water (associated or dissociated) with coverage, but instead the changes occur in the non-interacting bond distances. For molecular water, there is a decrease of 0.24 Å in the bond distance between one of the H atoms on H_2O and the adjacent O_x atom (O_x—H_1) and the O_w—Ti bond distance shrinks by 0.06 Å. These changes again reflect the increase in the strength of the water–surface interactions for the molecular configuration with decreasing coverage. For the dissociated water on TiO_2 termination, there is a similar decrease in the O_w—Ti bond. But the more important effect of the lower coverage is made clear by comparing Figures 4(d) and 3(d) that represent the dissociated minima at 1/8 and 1/2 ML, respectively. At 1/2 ML coverage, the two hydroxyl groups (O_x—H and O_w—H) are restricted in the ability to relax to optimise the interaction due to the presence of hydroxyl groups on both sides. This restriction is lifted at 1/8 ML and as can be seen in Figure 4(d), the two hydroxyl groups relax and rotate away from each other. The net effect of this additional relaxation is an increase in the stability of the dissociated H_2O molecule at the lower coverage.

To probe the observed crossover in the preferred structure of water, we examined 1/8, 1/4, 3/8 and 1/2 ML coverages on the 2×2 surface cell. The use of the 2×2 surface cell also allows us to study any size effects due to periodic boundary conditions at 1/2 ML. Figure 5 plots the adsorption energy of the most favoured configuration identified as a function of coverage (ML) on the 2×2-TiO_2 termination along with the earlier values at 1/2 ML

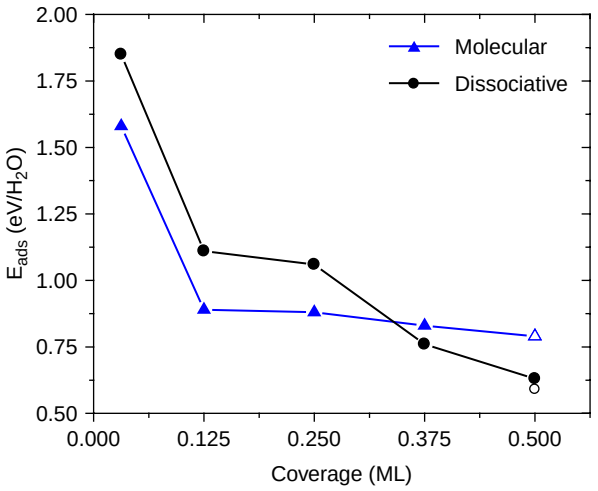

Figure 5. E_{ads} of the most favoured molecular (triangle) and dissociative (circle) water configuration at varying coverages on the 2×2-TiO_2 termination. The adsorption energies for the molecular and dissociated H_2O on the 1×1-TiO_2 termination are included as open symbols at 1/2 ML.

found on the 1×1-TiO_2 termination. Figure 6(a)–(c) illustrates the relaxed dissociative water at 1/4 ML coverage (2 water molecules/2×2 surface unit cells) in three different possible adsorbate configurations. The configurations vary in the distance between water molecules (Figure 6(a) vs. Figure 6(b),(c)) or the relative orientation (Figure 6(b) vs. Figure 6(c)). We have also examined water binding molecularly for each of these three configurations. For molecular binding, the adsorbed water interacts similarly for all of the configurations with E_{ads} of 0.82, 0.88 and 0.88 eV/H_2O, for molecular equivalents of the dissociative configurations in Figure 6(a)–(c), respectively. However, for dissociative binding, there are significant variations in the adsorption energy with surface configuration with an E_{ads} of 1.02, 1.06 and 0.56 eV/H_2O in Figure 6(a)–(c), respectively. The reason for this significant reduction in E_{ads} for the configuration shown in Figure 6(c) is due to repulsive interactions between the O_x—H and the O_w—H groups. The unfavourable configuration associated with Figure 6(c) is similar to the configuration we find for 1/2 ML on the 1×1 surface cell (see Figure 3(c)). At a coverage of 1/4 ML, the water adsorbates can avoid this unfavourable interaction by taking on configurations as shown in Figure 6(a),(b), which allow for rotations of the two adjacent hydroxyl groups. However, the addition of one more water molecule to the surface in any surface site will create this unfavourable row of hydroxyl groups that are restricted by having two neighbours on either side. Therefore, at 3/8 ML coverage, the molecular water state is favoured over dissociative adsorption, as illustrated by the E_{ads} in Figure 5 where we observe that the crossover

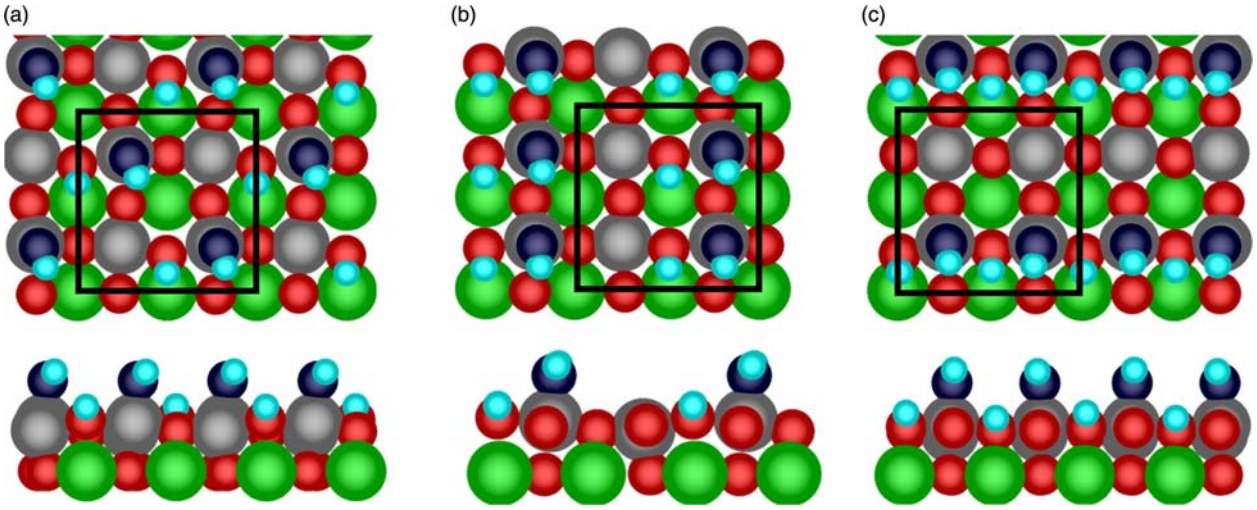

Figure 6. The three possible configurations of dissociatively adsorbed water at 1/4 ML coverage on the 2×2-TiO_2 termination viewed along the [001] and [100] directions with E_{ads} values of (a) 1.02, (b) 1.06 and (c) 0.56 eV/H_2O. The 2×2 surface unit cell is outlined by the solid box for visual aid of the top view along the [001] direction.

to favourability of dissociative water occurs at coverages below 3/8 ML.

Using the 2×2 surface unit cell, we also revisited the favoured configurations found on 1×1-TiO_2 termination. For the dissociative state at 1/2 ML on the 2×2-TiO_2, the *cis*-type hydroxyl group configuration binds with slightly higher adsorption energy of 0.63 eV/H_2O than the *trans*-type hydroxyl group configuration found on the 1×1-TiO_2 termination with an adsorption energy of 0.59 eV/H_2O (see Figure 5 at 1/2 ML). The adsorbate configuration on the 2×2-TiO_2 termination is mediated by surface TiO_6 octahedral rotation. Periodic boundary conditions restrict this tilting in the 1×1-TiO_2 system, thus reflecting the lower adsorption energy. Figure 7 isolates the top layer of TiO_6 octahedral in order to aid in visualisation of this tilting. This tilting occurs because at this coverage, oxygen within each hydroxyl group binds to a surface Ti atom and thereby completes the octahedral coordination. The hydrogen freed from each water molecule then binds to the neighbouring surface oxygen and triggers a buckling up or down of the surface oxygen and results in each octahedral rotation. Specifically, the Ti atom buckles up by about 0.2 Å, while the oxygen atoms buckle up by 0.31 or down by 0.23 Å. In addition to the buckling normal to the surface, in the top view shown in Figure 7, there is movement of the oxygen perpendicular to the surface normal direction. We tested the role of the surface response by fixing the surface atoms to the ideal (optimised bare surface) position and examining both molecular and dissociated water at 1/8 ML coverage on the 2×2 TiO_2 surface. We found the dissociated water recombines to the molecular state. With the molecularly bound water, the E_{ads} on the fixed surface is reduced by 0.30 eV/H_2O with respect to the 1/8 ML molecular state.

Similar to the 2×2-TiO_2 termination, we examined different configurations at 1/4 ML on the 2×2-SrO terminated surface. The configurations for dissociated water following relaxation are shown in Figure 8(a)–(c) with an adsorption energies of 1.01, 1.22 and 1.20 eV/H_2O, respectively. Molecular water in similar configurations shown in Figure 8(a)–(c) binds with adsorption energies of 0.85, 0.70 and 0.76 eV/H_2O and therefore, as at 1/8 ML, the dissociated water configurations will be favoured at 1/4 ML on the SrO termination.

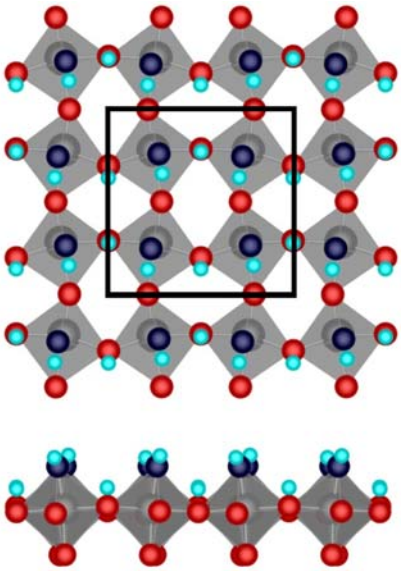

Figure 7. Top layer of TiO_6 octahedral for the 2×2 surface unit cell of TiO_2 terminated with 1/2 ML of dissociated water on the Ti site viewed along the [001] (top) and [100] (bottom). The 2×2 surface unit cell is outlined by the solid box for visual aid of the top view along the [001] direction.

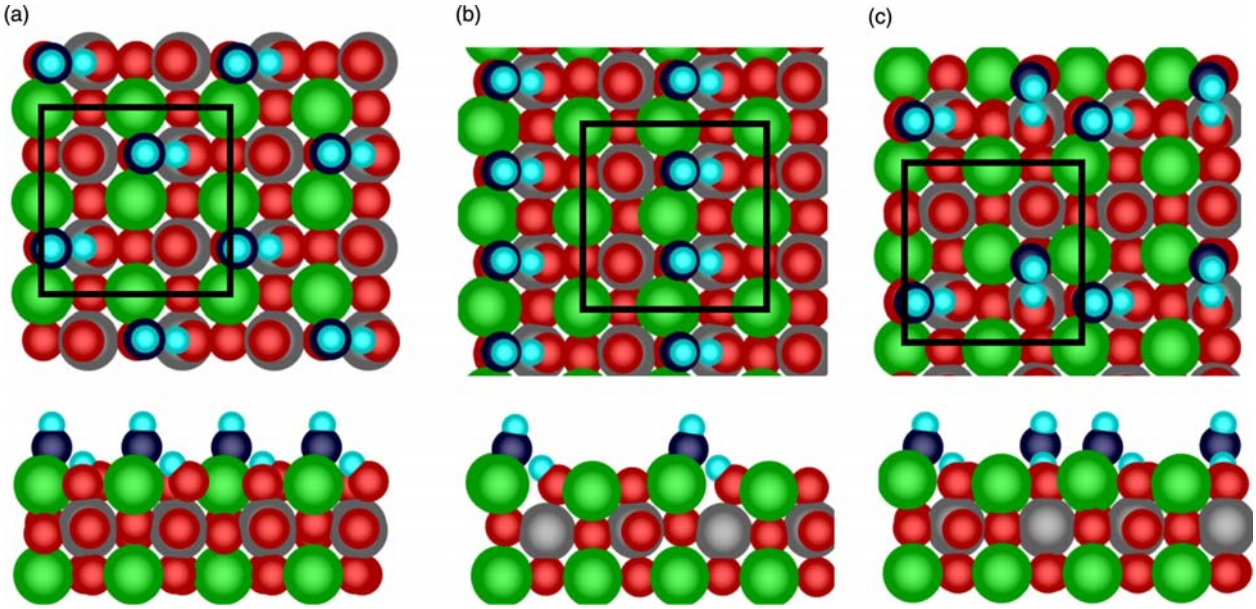

Figure 8. The three possible configurations of dissociatively adsorbed water at 1/4 ML coverage on the 2×2-SrO termination viewed along the [001] and [100] directions with E_{ads} values of (a) 1.01, (b) 1.22 and (c) 1.20 eV/H_2O. The 2×2 surface unit cell is outlined by the solid box for visual aid of the top view along the [001] direction.

Unlike on TiO_2, the adsorption energy for dissociated H_2O only slightly decreases (0.1–0.3 eV/H_2O) with respect to the favoured dissociated configuration at 1/8 ML, ($E_{ads} = 1.31$ eV/H_2O). Additionally, the configuration that was found to be least stable on the TiO_2 termination (Figure 6(c)) is found to be the most stable on the SrO termination (Figure 8(c)). In Figure 8(c), we see the dissociated hydroxyl groups seem to cluster instead of lining up in a row along the surface cations as was seen in Figure 6(c). This clustering is due to the favoured adsorption site of the hydroxyl group at 1/4 ML on the SrO termination, namely a transition from a bridge to a fourfold type site as illustrated in Figure 2(a). Within the primitive 1×1 unit cell of the SrO termination, there are two equivalent fourfold sites. The close proximity of the second fourfold site allows one of the dissociated water groups to rotate the hydroxyl portion to the neighbouring fourfold site and away from the initial fourfold site, which was aligned along the [010] direction. At 3/8 ML, we find an adsorption energy for the dissociated water of 1.12 eV/H_2O, which is less stable by 0.19 eV to that determined at 1/8 ML. The molecular water configuration has an adsorption energy of 0.71 eV/H_2O and therefore at 3/8 ML as at 1/4 and 1/8 ML, the dissociated water configuration is favoured on the SrO termination. Finally, at 1/2 ML coverage, we see some repulsive interactions between the adsorbates with an adsorption energy of 0.97 eV/H_2O and the recombination of one of the water molecules resulting in a mixed adsorption configuration. We did identify a pure molecular configuration with the H_2O molecules sitting on the fourfold sites. This configuration had an adsorption energy of 0.64 eV/H_2O, compared to a value of 0.58 eV/H_2O on the 1×1 surface cell. This slight increase can be attributed to the ability of the water molecules to take on alternative up and down orientation (not shown), which slightly stabilises the molecular water layer. Nevertheless, by comparing the adsorption energy of the mixed adsorption configuration (0.97 eV/H_2O) with molecular water on the bridge site of the 1×1 SrO (0.84 eV/H_2O) or at the fourfold sites of the 2×2 SrO (0.64 eV/H_2O), we find that the mixed configuration is favoured. The mixed adsorbate configuration on the 2×2-SrO surface, the inability to stabilise water molecules on the bridge sites on the 2×2-SrO surface and the observed octahedral tilting of the TiO_6 octahedral of the 2×2-TiO_2 surface indicate that for even high coverages, a minimum 2×2 surface unit cell is needed to fully probe the structure of water due to these subtle adsorbate–adsorbate interactions. If the DFT-predicted configurations at 1/2 ML are accurate, they suggest that LEED probing the water layers on $SrTiO_3$(100) should show doubling of the unit cell.

Utilising the code of Henkelman et al. [37] and Sanville et al. [38], we determined the Bader charges based on the Bader criteria for decomposing the electron density [39]. Table 3 summarises the Bader charges for the 1×1 and 2×2 surface unit cells of both the SrO and TiO_2 terminations. In each case, the hydrogen atom is assigned zero electrons according to the Bader criteria due to the lack of zero-flux surfaces in the electron density gradient between the hydrogen and oxygen atoms. Although not shown, the electron charge density was examined

Table 3. The average Bader atomic charges in units of *e* for Sr, Ti, H and O within the oxide and water are shown for molecular and dissociative water on both TiO_2 and SrO terminations.

	TiO_2 termination		SrO termination	
	Molecular (1/8, 1/4, 1/2)	Dissociative (1/8, 1/4, 1/2)	Molecular (1/8, 1/4, 1/2)	Dissociative (1/8, 1/4, 1/2)
Sr	1.58	1.58	1.60	1.60
Ti	2.14	2.14	2.16	2.14
O_{surf}	−1.24	−1.24 (−1.67)	−1.24	−1.23 (−1.77)
O_{water}	−1.97	−1.53	−2.09	−1.78
H	1.00	1.00	1.00	1.00

Note: For the dissociative adsorption, the surface oxygen bound to the free hydrogen is distinguished in parentheses.

to confirm the lack of a gradient between hydrogen and oxygen. Therefore, the hydrogen atom's electron is assigned to the bonding oxygen. This is evident by the significant change in charge associated with the terminal oxygen before and after dissociation. After dissociation, the water oxygen loses 0.44 (0.31) electrons on the TiO_2 (SrO) termination and the surface oxygen bound to the free hydrogen gains 0.43 (0.54) electrons. Though the Bader charges determined in our study underestimate the ionic character of both the Sr and Ti atoms with respect to that determined by Evarestov et al. [21], the general features agree well. Similar to Evarestov et al., we determine that the Sr, Ti and O (not bound to the free hydrogen) charges are unaffected by the dissociation of water [21]. On both terminations, the charges are unaffected by changes in coverage or surface unit cell, e.g. 1/2 ML molecular water on 1×1 TiO_2 has the same charges as 1/2 and 1/8 ML molecular water on 2×2 TiO_2. This observation suggests that the observed changes in stability of coverage are not linked with changes in bonding, but instead are dependent on electrostatic interactions. Calculations with larger unit cells (4×4) would also be useful in determining the role of long-range substrate-mediated interactions vs. electrostatic interactions, but we leave such analysis to future studies.

The larger charge transfer on the SrO termination can help examine the clustering effect observed on the 2×2 SrO surface with 1/4 ML coverage, illustrated in Figure 8(c). The initial configuration, with the two dissociated water groups aligning along the surface Sr cations, places each hydroxyl group between two surface oxygen bound to two free hydrogen atoms. Since each of these surface oxygen atoms gain 0.54 electrons following adsorption of free hydrogen atoms, each of the two surface oxygen atoms would have a charge of $-1.7e$. The two hydroxyl groups from the two adsorbed water would also have a charge of $-1.7e$. The close proximity of these charges would lead to significant repulsion between the surface- and water-based hydroxyl groups. This repulsion in combination with the close proximity of another free favourable surface adsorption site on the 2×2 surface leads to the rotation previously mentioned.

3.3 *Vibrational modes of $H_2O/SrTiO_3(100)$*

A useful experimental probe in attempting to resolve between molecular vs. dissociated water is HREELS or other vibrational spectroscopy tools [17,18]. Lopez et al. [16] reported vibrational spectra of water on both clean and sodium-modified $SrTiO_3(100)$ at room temperature. The absence of the OH band at $3600\,cm^{-1}$ indicated that water did not adsorb on clean $SrTiO_3$ but this is likely due to the experiments being performed at room temperature. Wang et al. [7] in their TPD study demonstrated that lower temperatures are needed to have uptake of H_2O on pristine $SrTiO_3(100)$. However, after sodium atoms are co-adsorbed with water on the $SrTiO_3(100)$, a feature was observed at $3660\,cm^{-1}$, attributed to the OH band [16]. This feature was independent of the water exposure indicating surface saturation at low water exposure. Though not discussed, the absence of a feature near $1595\,cm^{-1}$ would indicate that water was adsorbed dissociatively, as this feature is attributed to H—O—H bond angle scissoring. Cox et al. [11] completed an HREELS study of water adsorption on $SrTiO_3(100)$ at 100 K and found two main peaks associated with a moderate dosage (four Langmuir) of water, a sharp peak at $3662\,cm^{-1}$ and another peak at $1686\,cm^{-1}$. Cox et al. attributed the high-frequency mode to symmetric stretching of the OH bond and the low-frequency mode to the bond angle bending mode, thereby concluding that water binds molecularly on pristine $SrTiO_3$. However, due to a poor noise to signal ratio, the asymmetric OH stretching mode was not resolved. Overall, while there have been vibrational studies of $H_2O/SrTiO_3(100)$, the coverage in these studies is not known and full mode assignment, including resolving shifts of frequencies upon adsorption, has not been made.

We used DFT to determine the vibrational modes of the most stable dissociative and molecular water structure at 1/8 ML on the SrO and TiO_2 termination. To allow for a computationally tractable but accurate evaluation of the vibrational modes associated with the water adsorbate and its interaction with the surface, we fixed the oxide atoms not participating directly in the water adsorption. A finite central difference method with a displacement of 0.05 Å

is used to calculate the Hessian matrix. Neglecting the surface modes, the zero point corrections (ZPC) to the adsorption energy are 0.056 and 0.092 eV/H_2O molecule for the 0.125 ML coverage dissociative and molecular state on the TiO_2 termination, respectively. These corrections are not sufficient to change the favourability of the dissociative state over the molecular state and therefore do not affect our primary conclusions and ZPC adsorption energies are not reported in this paper. The frequencies and mode assignments are summarised in Table 4. The mode associated with stretching of the H—O bond is split for molecular water on the TiO_2 termination. The hydrogen oriented away from the surface oxide (i.e. H_1 in Tables 2 and 4) has the characteristic frequency of 3609 cm^{-1} (3666 cm^{-1}), while the hydrogen oriented towards the oxide (i.e. H_2) is assigned a frequency nearly 300 cm^{-1} lower at 3337 cm^{-1} (3254 cm^{-1}) at 1/8 ML (1/2 ML) coverage. The bond angle scissoring mode has a frequency of 1585 and 1571 cm^{-1}, for the 1/8 and 1/2 ML coverage, respectively, which is very near the expected 1595 cm^{-1}. The dissociatively bound water at 1/8 ML has vibrational modes of 3762 and 3644 cm^{-1} associated with O—H stretching of the water hydroxyl group and surface oxide, respectively. The same modes for the 1/2 ML coverage are slightly down shifted at 3734 and 3513 cm^{-1}. At either coverage, the low-frequency mode near 1595 cm^{-1} was not observed due to the loss of the H—O—H bond angle scissoring.

Onal et al. [40] computationally investigated water adsorption on small clusters representative of (101) and (100) surfaces of anatase TiO_2 structure. Vibrational frequencies determined compare well to available experimental data. Similar to our findings, there were marked differences between the frequencies associated with molecular and dissociative adsorption. On (101) TiO_2, molecular adsorption exhibited three features at 3005, 3661 and 1605 cm^{-1} and dissociative adsorption only two at 3666 and 3713 cm^{-1}. The dissociated water on TiO_2(101) frequencies are within 50 cm^{-1} to those determined on the TiO_2-terminated $SrTiO_3$(100) surface. For the molecular state on TiO_2(101), there is also a downward shift in the frequency of the O—H stretching mode by 600 cm^{-1} similar to that observed on $SrTiO_3$(100) but with larger magnitude.

The vibrational modes of molecular and dissociative water at 1/8 ML on the 2 × 2-SrO surface and 1/2 ML on the 1 × 1-SrO surface are included in Table 4. For dissociative water at 1/8 ML, the hydrogen–oxygen stretching within the dissociated hydroxyl group has an upward shift in frequency to 3788 cm^{-1} vs. the same mode on the 2 × 2-TiO_2 surface at a frequency of 3762 cm^{-1}. The dissociated hydrogen to surface oxygen stretching is significantly altered on the 2 × 2-SrO surface (2864 cm^{-1}) vs. 2 × 2-TiO_2 surface (3644 cm^{-1}). The change in this mode between the two surfaces is related to the adsorbate structures and adsorption sites. On the TiO_2 termination, the dissociated hydrogen stretches into the free space above the surface. In the fourfold adsorption site on the SrO termination, the dissociated hydrogen stretches between the surface oxide and the oxygen from the dissociated water. Additional modes not observed on the TiO_2 termination are identified on both the 1 × 1- and 2 × 2-SrO surfaces due to the open nature of the SrO surface plane. The dissociated hydrogen stretches into the open fourfold high symmetry site (see Figure 2(a)). This stretching results in a pseudo bond angle bending mode with two frequencies of 1111 and 1047 cm^{-1} at 1/8 ML on 2 × 2 SrO and three frequencies of 1543, 1345 and 1251 cm^{-1} at 1/2 ML on 1 × 1 SrO. These low-frequency

Table 4. DFT-derived vibrational frequencies in cm^{-1} of isolated water, molecular and dissociative water at the favoured site on the 2 × 2 and 1 × 1 SrO and TiO_2 termination and the corresponding mode assignment.

	Frequency (cm^{-1})	Mode assignment
Isolated H_2O		
H—O_w	3838 (3756)	Asymmetric stretching
H—O_w	3723 (3657)	Symmetric stretching
H—O_w—H	1560 (1595)	Bending (scissoring)
1/8 ML H_2O on 2 × 2 TiO_2		
H_1—O_w	3609	Asymmetric stretching
H_2—O_w	3337	Asymmetric stretching
H_1—O_w—H_2	1585	Bending (scissoring)
1/8 ML H—OH on 2 × 2 TiO_2		
H_1—O_w	3762	Stretching
H_2—O_x	3644	Stretching
1/2 ML H_2O on 1 × 1 TiO_2		
H_1—O_w	3666	Asymmetric stretching
H_2—O_w	3254	Asymmetric stretching
H_1—O_w—H_2	1571	Bending (scissoring)
1/2 ML H—OH on 1 × 1 TiO_2		
H_1—O_w	3734	Stretching
H_2—O_x	3513	Stretching
1/8 ML H_2O on 2 × 2 SrO		
H_1—O_w—H_2	2593	Symmetric stretching
H_1—O_w—H_2	2542	Asymmetric stretching
H_1—O_w—H_2	1546	Bending (scissoring)
H_1—O_w—H_2	1248	Pseudo-bending (scissoring)
1/8 ML H—OH on 2 × 2 SrO		
H_1—O_w	3788	Stretching
H_2—O_x	2864	Stretching
H_1—O_w—H_2	1111	Pseudo-bending (scissoring)
H_1—O_w—H_2	1047	Pseudo-bending (scissoring)
1/2 ML H_2O on 1 × 1 SrO		
H_1—O_w	3780	Asymmetric stretching
H_2—O_w	2118	Asymmetric stretching
H_1—O_w—H_2	1579	Bending (scissoring)
H_1—O_w—H_2	1113	Pseudo-bending (scissoring)
1/2 ML H—OH on 1 × 1 SrO		
H_1—O_w	3785	Stretching
H_1—O_w—H_2	1543	Pseudo-bending (scissoring)
H_1—O_w—H_2	1345	Pseudo-bending (scissoring)
H_1—O_w—H_2	1251	Pseudo-bending (scissoring)

Note: For isolated H_2O, the experimental values [10] are given in parentheses.

pseudo-bending modes are also observed for the molecular states on both 1×1 and 2×2 SrO. For 1/2 ML, the expected O_w—H stretching has a frequency of 3780 and 2118 cm^{-1}, the bond angle bending mode at 1579 cm^{-1} and one pseudo bond angle bending mode at 1113 cm^{-1}. At 1/8 ML, the molecular water adsorbed in the fourfold site leads to a downshift in the frequencies. Symmetric stretching of the water hydrogen atoms has a frequency of 2593 cm^{-1} vs. the isolated water mode at 3838 cm^{-1}. The asymmetric stretching of the hydrogen atoms is 2542 cm^{-1}, nearly 1200 cm^{-1} shift in the mode. The bond angle bending mode has a frequency of 1546 cm^{-1} similar to the isolated molecule at 1560 cm^{-1}. The pseudo bond angle bending occurs at 1/8 ML as well but at a frequency of 1248 cm^{-1} vs. 1113 cm^{-1}. Despite this pseudo bond angle bending, the $\sim$400 cm^{-1} downward shift in the frequency should be sufficiently large to distinguish between a dissociatively or molecularly bond water at a given coverage on the SrO termination of $SrTiO_3$(100). However, care must be taken in identifying the coverage of water on the surface since the pseudo-bending mode at 1/8 ML molecular water on SrO (1248 cm^{-1}) is nearly the same as that of 1/2 ML dissociative water on SrO (1251 cm^{-1}).

As mentioned in the introduction, water adsorption on MgO (100) has been extensively studied with varying results. Chizallet et al. [41] examined IR features of OH groups on MgO using both cluster and periodic DFT calculations. The vibrational modes determined were compared to experimental spectra showing a broad low-frequency feature between 3200 and 3650 cm^{-1} and a sharp high-frequency feature between 3650 and 3800 cm^{-1}. The theoretical investigation identified various features based on the water adsorbate configuration, providing some insight into the broad low-frequency feature. Lower frequency modes around 1800 cm^{-1} are associated with H—O—H bending modes for the 'slightly' dissociated water molecule, similar to observations made here.

3.4 Discussion on potential sources of DFT-experiment disagreement

In the introduction, we discussed the experimental studies that conclude the presence of only molecular water on pristine $SrTiO_3$(100). The only study of water at low coverages is the TPD study of Wang et al. [7], and while they see peak temperatures close to 260 K, which is associated with molecular H_2O, there is no direct evidence, for example from HREELS vibrational spectra or scanning tunnelling microscope (STM) images of the state of H_2O at low coverages vs. at high coverages. As noted earlier, conflicting models between DFT and experiment in the resolution of structure of water on oxide surfaces is not new, as in both TiO_2(110) and MgO(100) there has been initial disagreement. Below, we address some possible sources of the difference between our DFT results and experimental studies.

3.4.1 Evaluation of the exchange-correlation functional

One often raised concern with DFT studies is the impact of the functional on the accuracy of the calculations. Could the favourability of dissociated H_2O found in our calculations be due to error associated with the PBE functional? There are numerous DFT studies of water adsorption on various oxide surfaces [5,40,42,43], including the discussed HF-DFT study of H_2O/$SrTiO_3$(100) [21], which suggest in general that GGA-type functional will more accurately describe H_2O adsorption than the LDA functional. Nevertheless, within GGA, there are several different implementations and hybrid functionals, such as PBE0 [44,45] and HSE06 [46,47] that are expected to be more accurate than PBE. At least one drawback to the hybrid functionals is the additional computational expense in their current implementation in plane-wave codes such as VASP [48,49]. To characterise the error in the GGA-PBE calculations reported in this paper, we have repeated select calculations with other GGA functionals. Table 5 shows the bulk $SrTiO_3$ lattice parameter and the adsorption energy at a coverage of 1/8 ML on the TiO_2-terminated $SrTiO_3$(100) surface for both associated and dissociated H_2O. We have focused the testing of the functional on TiO_2 termination, since the experimental $SrTiO_3$(100) surface is expected to be dominated by this termination [7]. PBEsol and the two hybrid functionals reproduce the experimental lattice parameter value of 3.90 Å precisely, while the PBE and revised Perdew–Burke–Ernzerhof (RPBE) functionals are less accurate with values of 3.95 and 3.98 Å, respectively. These results match with earlier studies that have shown that PBEsol is very effective in capturing the bulk structure without the expense of the hybrid functionals [33,49]. Unfortunately, applying the PBEsol to calculate the adsorption energy gives values that are nearly double the PBE results, a trend that matches earlier tests of this functional [49], but even within PBEsol

Table 5. Bulk lattice parameter (Å) of $SrTiO_3$ and the adsorption energy (eV/H_2O) for molecular and dissociative H_2O at 1/8 ML on the TiO_2-terminated $SrTiO_3$(100) surface for various exchange-correlation functionals.

Functional	Lattice parameter	E_{ads} (molecular)	E_{ads} (dissociated)
PBE	3.95	0.89	1.11
RPBE	3.98	0.84	1.13
PBEsol	3.90	2.67	2.83
PBE0	3.90	–	–
HSE06	3.90	–	–
Experiment	3.90	–	–

the dissociated structure is favoured. The RPBE functional gives very similar results as PBE and most importantly confirms the preference for dissociated water at low coverages. Unfortunately, we were not able to perform similar tests of the adsorption energies using the hybrid functional due to the computational expense. Future testing with a more computationally tractable system (i.e. Γ-point and thinner slabs) will help to clarify any quantitative changes to the adsorption energy, but we do not expect a reversal of the favourability of the water structure using the hybrid functionals due to the large energy difference (~0.20 eV) between the two structures in our PBE-DFT calculations.

3.4.2 *Clustering effects – favoured dimer configurations*

Clustering of water molecules could dramatically affect the stable structures on the surface. For example, co-adsorbed HO—H_2O complexes have been identified on PdO(101) [43], TiO_2(011) [50], TiO_2(110) [51] and MgO(001) [4,52]. While a thorough study of cluster effects on the structure and stability of water on $SrTiO_3$(100) is beyond the scope of this paper, we have attempted to determine stable dimer configurations on the 2×2-TiO_2 termination. The goal is to probe on the 2×2 surface unit cell if any dimer complexes (H_2O—H_2O, OH—OH or HO—H_2O) are more favoured over the isolated dissociated water structure identified at 1/4 and 1/8 ML. We used the stabilised molecular and dissociative water structure at 1/8 ML from Section 3.2 and added molecular water to neighbouring high symmetry sites from Figure 2. We found when molecular water is added near the dissociated water either the dissociative water recombines or the molecular water shifts over to the next bridge site, thereby increasing the interatomic distance. For most of the configurations with two molecular water adsorbates, the two molecules separate in order to increase the interatomic distance between molecules to a state similar to the molecular equivalent of configuration in Figure 6(c). In one case, the second water adsorbs to the neighbouring fourfold site, see Figure 2(h), and orients itself perpendicular to the original state with one hydrogen pointed towards the surface and one pointed away. For each of these configurations, the total adsorption energy is found to be between 0.11 and 0.16 eV/H_2O, less favoured than the molecular equivalent shown in Figure 6(c). Therefore, these configurations do not stabilise dissociative adsorption and on the 2×2-TiO_2 termination the isolated dissociated H_2O remains the most favoured configuration we have identified. However, the cluster configuration of molecular water adsorbed to the bridge and fourfold site provides some insight into how the TiO_2 termination may favourably accommodate surface saturation at high coverages of 1 ML. While our initial study of dimer configurations has not found any favoured clustering on the TiO_2 termination, future studies using larger surface unit cells and probing more configurations for stable clusters of water molecules would assist in more firmly resolving the role of intermolecular interactions of water on the $SrTiO_3$(100) surface.

3.4.3 *Kinetic barrier to dissociation*

One potential scenario that would resolve the difference between DFT and experiment is the presence of an energy barrier to dissociation of H_2O on the surface that is larger than the desorption energy. Under these conditions, the molecular state would be kinetically trapped. We first used the NEB method to identify the barrier on the 1×1-SrO and TiO_2 termination. For the 1×1-SrO surface, the energy difference between the molecular and dissociative states was 0.01 eV (see Table 1). Both the barrier to dissociation and association on the 1×1-SrO termination are negligible at 0.00 and 0.05 eV, respectively. On the 1×1-TiO_2 termination surface, where the molecular water is favoured, the dissociation (association) barrier is 0.29 (0.13) eV. Both these barriers are relatively small in comparison with the adsorption energies and would suggest that kinetic barriers will not play a large role in the observed species on the surface. Nevertheless, the crossover to dissociated water occurs at lower coverages and, therefore, we evaluated the energy barrier on the 2×2 TiO_2 at a coverage of 1/8 ML to examine both the role of system size and adsorbate coverage. The *cis*-type dissociative structure was used in order to compare with the results for the 1×1-TiO_2 system. Additionally, to reduce the computational expense, the force criterion was slightly reduced for the NEB calculations from 0.03 to 0.05 eV/Å. The resulting dissociation barrier is 0.08 eV, while recombination has a barrier of 0.34 eV. Therefore, the dissociation barrier in fact becomes smaller and is negligible at lower coverages. While not explicitly calculated for the 2×2-SrO termination, we would expect similar results for the dissociation barrier. These calculated energy barriers suggest that the discrepancy between DFT and experimental observations cannot be resolved by invoking large kinetic barriers to dissociations.

4. Conclusions

The stability of molecular vs. dissociated water as a function of coverage on both terminations of $SrTiO_3$(100) was studied using DFT. At a coverage of 1/2 ML, we reproduce the general results of an earlier hybrid HF-DFT study [21], which predicts that associative H_2O will be the favoured structure on TiO_2 termination and negligible differences in stability between associative and dissociative H_2O on the SrO termination. Artificial size effects at coverages of 1/2 ML due to periodic boundary conditions were identified by comparison of 1×1 and 2×2 surface

unit cells. As the coverage is decreased below 3/8 ML, we find a crossover to dissociative water on the TiO_2 termination. On the 2×2-SrO termination, a mixed adsorbate structure can be stabilised at 1/2 ML and further decrease in coverage stabilises pure dissociative H_2O. The DFT results reported in this paper at lower coverages conflict with the general conclusions of experiments examining $H_2O/SrTiO_3(100)$, but these experiments have not yet presented a fully detailed picture of water on $SrTiO_3(100)$. It remains an open question of the source of the differences between our DFT results and the experimental studies. We have probed possible stabilisation mechanisms for molecular water, but we do not find that clustering or kinetic barriers to dissociation leads to additional stabilisation of molecular over dissociated water. A possibility that would dramatically affect the comparison between experiment and DFT would be adsorbate-induced surface reconstructions. As noted in the introduction, the experimental studies note a unreconstructed 1×1-$SrTiO_3$ surface, but several studies have shown that there are numerous reconstructions for $SrTiO_3(100)$ and the surface structure is sensitive to both the environment and preparation [53,54]. The TPD study of H_2O on $SrTiO_3(100)$ does report LEED patterns before the water exposure indicates a 1×1 unreconstructed surface [7], but it did not probe the surface structure during and after exposure to H_2O. The $SrTiO_3$ surface could reconstruct upon adsorption, which would lead to different surface–adsorbate interactions and under that scenario, our DFT study would not be examining the relevant configurations. To probe possible reconstructions upon H_2O adsorption would be non-trivial using DFT without any input from experiment. Future experimental studies that probe the surface structure during water exposure, for example with STM, would be critical to resolve the role of clustering and/or ordering of water and any possible adsorbate-induced reconstructions. DFT studies to elucidate the role of O vacancies and step edges on water structure, in particular vibrational modes specific to these defects, would assist in the interpretation of experimental data. Such combined DFT-STM studies have been critical, for example to resolve the water structure on $TiO_2(011)$ [50] and we expect the results reported in this paper will motivate similar studies on $SrTiO_3(100)$.

Acknowledgements

We gratefully acknowledge the financial support for this work provided by the National Science Foundation under NSF CHE Grant #0911553. We also acknowledge the University of Florida High-Performance Computing Center (http://www.hpc.ufl.edu) for providing computational resources for performing the calculations reported in this paper.

References

[1] M.A. Henderson, *The interaction of water with solid surfaces: Fundamental aspects revisited*, Surf. Sci. Rep. 46 (2002), pp. 5–308.
[2] U. Diebold, *The surface science of titanium dioxide*, Surf. Sci. Rep. 48 (2003), pp. 53–229.
[3] F. Allegretti, S. O'Brien, M. Polcik, D.I. Sayago, and D.P. Woodruff, *Adsorption bond length for H_2O on $TiO_2(110)$: A key parameter for theoretical understanding*, Phys. Rev. Lett. 95 (2005), 226104.
[4] Y.D. Kim, J. Stultz, and D.W. Goodman, *Dissociation of water on MgO(100)*, J. Phys. Chem. B 106 (2002), pp. 1515–1517.
[5] L. Giordano, J. Goniakowski, and J. Suzanne, *Reversibility of water dissociation on the MgO (100) surface*, Phys. Rev. B 62 (2000), pp. 15406–15408.
[6] M.A. Johnson, E.V. Stefanovich, T.N. Truong, J. Gunster, and D.W. Goodman, *Dissociation of water at the MgO(100)–water interface: Comparison of theory with experiment*, J. Phys. Chem. B 103 (1999), pp. 3391–3398.
[7] L.Q. Wang, K.F. Ferris, and G.S. Herman, *Interactions of H_2O with $SrTiO_3(100)$ surfaces*, J. Vacuum Sci. Technol. A: Vacuum Surf. Films 20 (2002), pp. 239–244.
[8] N.B. Brookes, G. Thornton, and F.M. Quinn, *$SrTiO_3(100)$ step sites as catalytic centers for H_2O dissociation*, Solid State Commun. 64 (1987), pp. 383–386.
[9] N.B. Brookes, F.M. Quinn, and G. Thornton, *The involvement of step and terrace sites in H_2O adsorption on $SrTiO_3(100)$*, Phys. Scr. 36 (1987), pp. 711–714.
[10] R.G. Egdell and P.D. Naylor, *The adsorption of water on $SrTiO_3(100)$ – A study by electron-energy loss and photoelectron spectroscopies*, Chem. Phys. Lett. 91 (1982), pp. 200–205.
[11] P.A. Cox, R.G. Egdell, and P.D. Naylor, *HREELS studies of adsorbates on polar solids – Water on $SrTiO_3(100)$*, J. Electron Spectrosc. Relat. Phenom. 29 (1983), pp. 247–252.
[12] S. Eriksen, P.D. Naylor, and R.G. Egdell, *The adsorption of water on $SrTiO_3$ and TiO_2 – A reappraisal*, Spectrochim. Acta Part A Mol. Biomol. Spectros. 43 (1987), pp. 1535–1538.
[13] C. Webb and M. Lichtensteiger, *UPS/XPS study of reactive and non-reactive $SrTiO_3$ (100) surfaces – Adsorption of H_2O*, Surf. Sci. 107 (1981), pp. L345–L349.
[14] M.S. Wrighton, A.B. Ellis, P.T. Wolczanski, D.L. Morse, H.B. Abrahamson, and D.S. Ginley, *Strontium titanate photoelectrodes. Efficient photoassisted electrolysis of water at zero applied potential*, J. Am. Chem. Soc. 98 (1976), pp. 2774–2779.
[15] M. Woodhouse and B.A. Parkinson, *Combinatorial approaches for the identification and optimization of oxide semiconductors for efficient solar photoelectrolysis*, Chem. Soc. Rev. 38 (2009), pp. 197–210.
[16] A. Lopez, T. Heller, T. Bitzer, Q. Chen, and N.V. Richardson, *The influence of sodium on the adsorption of water on $SrTiO_3(100)$-1×1 surfaces*, Surf. Sci. 494 (2001), pp. L811–L814.
[17] M.A. Henderson, *Structural sensitivity in the dissociation of water on TiO_2 single-crystal surfaces*, Langmuir 12 (1996), pp. 5093–5098.
[18] M.A. Henderson, *An HREELS and TPD study of water on $TiO_2(110)$: The extent of molecular versus dissociative adsorption*, Surf. Sci. 355 (1996), pp. 151–166.
[19] M.A. Henderson, *The influence of oxide surface structure on adsorbate chemistry: Desorption of water from the smooth, the microfaceted and the ion sputtered surfaces of $TiO_2(100)$*, Surf. Sci. 319 (1994), pp. 315–328.
[20] K.F. Ferris and L.-Q. Wang, *Electronic structure calculations of small molecule adsorbates on (110) and (100) TiO_2*, J. Vacuum Sci. Technol. A: Vacuum Surf. Films 16 (1998), pp. 956–960.
[21] R.A. Evarestov, A.V. Bandura, and V.E. Alexandrov, *Adsorption of water on (001) surface of $SrTiO_3$ and $SrZrO_3$ cubic perovskites: Hybrid HF-DFT LCAO calculations*, Surf. Sci. 601 (2007), pp. 1844–1856.
[22] G. Kresse and J. Hafner, Ab initio *molecular-dynamics for liquid-metals*, Phys. Rev. B 47 (1993), pp. 558–561.
[23] G. Kresse and J. Hafner, *Norm-conserving and ultrasoft pseudopotentials for first-row and transition-elements*, J. Phys.: Condens. Matter 6 (1994), pp. 8245–8257.

[24] G. Kresse and J. Hafner, Ab initio *molecular-dynamics simulation of the liquid-metal–amorphous-semiconductor transition in germanium*, Phys. Rev. B 49 (1994), pp. 14251–14269.

[25] G. Kresse and J. Furthmuller, *Efficient iterative schemes for* ab initio *total-energy calculations using a plane-wave basis set*, Phys. Rev. B 54 (1996), pp. 11169–11186.

[26] G. Kresse and D. Joubert, *From ultrasoft pseudopotentials to the projector augmented-wave method*, Phys. Rev. B 59 (1999), pp. 1758–1775.

[27] P.E. Blochl, *Projector augmented-wave method*, Phys. Rev. B 50 (1994), pp. 17953–17979.

[28] J.P. Perdew, K. Burke, and M. Ernzerhof, *Generalized gradient approximation made simple*, Phys. Rev. Lett. 77 (1996), pp. 3865–3868.

[29] M. Methfessel and A.T. Paxton, *High-precision sampling for Brillouin-zone integration in metals*, Phys. Rev. B 40 (1989), pp. 3616–3621.

[30] L. Bengtsson, *Dipole correction for surface supercell calculations*, Phys. Rev. B 59 (1999), pp. 12301–12304.

[31] H.J. Monkhorst and J.D. Pack, *Special points for Brillouin-zone integrations*, Phys. Rev. B 13 (1976), pp. 5188–5192.

[32] Y.L. Cao and Z.X. Chen, *Theoretical studies on the adsorption and decomposition of H_2O on Pd(111) surface*, Surf. Sci. 600 (2006), pp. 4572–4583.

[33] R. Wahl, D. Vogtenhuber, and G. Kresse, *$SrTiO_3$ and $BaTiO_3$ revisited using the projector augmented wave method: Performance of hybrid and semilocal functionals*, Phys. Rev. B 78 (2008), 104116.

[34] D. Sheppard, R. Terrell, and G. Henkelman, *Optimization methods for finding minimum energy paths*, J. Chem. Phys. 128 (2008), 134106.

[35] G. Henkelman and H. Jonsson, *Improved tangent estimate in the nudged elastic band method for finding minimum energy paths and saddle points*, J. Chem. Phys. 113 (2000), pp. 9978–9985.

[36] G. Henkelman, B.P. Uberuaga, and H. Jonsson, *A climbing image nudged elastic band method for finding saddle points and minimum energy paths*, J. Chem. Phys. 113 (2000), pp. 9901–9904.

[37] G. Henkelman, A. Arnaldsson, and H. Jonsson, *A fast and robust algorithm for Bader decomposition of charge density*, Comput. Mater. Sci. 36 (2006), pp. 354–360.

[38] E. Sanville, S.D. Kenny, R. Smith, and G. Henkelman, *Improved grid-based algorithm for Bader charge allocation*, J. Comput. Chem. 28 (2007), pp. 899–908.

[39] R. Bader, *Atoms in Molecules: A Quantum Theory*, Oxford University Press, New York, 1990.

[40] I. Onal, S. Soyer, and S. Senkan, *Adsorption of water and ammonia on TiO_2-anatase cluster models*, Surf. Sci. 600 (2006), pp. 2457–2469.

[41] C. Chizallet, G. Costentin, M. Che, F. Delbecq, and P. Sautet, *Infrared characterization of hydroxyl groups on MgO: A periodic and cluster density functional theory study*, J. Am. Chem. Soc. 129 (2007), pp. 6442–6452.

[42] A.V. Bandura, D.G. Sykes, V. Shapovalov, T.N. Troung, J.D. Kubicki, and R.A. Evarestov, *Adsorption of water on the TiO_2 (rutile) (110) surface: A comparison of periodic and embedded cluster calculations*, J. Phys. Chem. B 108 (2004), pp. 7844–7853.

[43] H.H. Kan, R.J. Colmyer, A. Asthagiri, and J.F. Weaver, *Adsorption of water on a PdO(101) thin film: Evidence of an adsorbed $HO–H_2O$ complex*, J. Phys. Chem. C 113 (2009), pp. 1495–1506.

[44] M. Ernzerhof and G.E. Scuseria, *Assessment of the Perdew–Burke–Ernzerhof exchange-correlation functional*, J. Chem. Phys. 110 (1999), pp. 5029–5036.

[45] C. Adamo and V. Barone, *Toward reliable density functional methods without adjustable parameters: The PBE0 model*, J. Chem. Phys. 110 (1999), pp. 6158–6170.

[46] J. Heyd, G.E. Scuseria, and M. Ernzerhof, *Hybrid functionals based on a screened Coulomb potential*, J. Chem. Phys. 118 (2003), pp. 8207–8215.

[47] O.A. Vydrov, J. Heyd, A.V. Krukau, and G.E. Scuseria, *Importance of short-range versus long-range Hartree–Fock exchange for the performance of hybrid density functionals*, J. Chem. Phys. 125 (2006), 249901.

[48] J. Hafner, Ab-initio *simulations of materials using VASP: Density-functional theory and beyond*, J. Comput. Chem. 29 (2008), pp. 2044–2078.

[49] A. Stroppa and G. Kresse, *The shortcomings of semi-local and hybrid functionals: What we can learn from surface science studies*, New J. Phys. 10 (2008), 063020.

[50] T.J. Beck, A. Klust, M. Batzill, U. Diebold, C. Di Valentin, A. Tilocca, and A. Selloni, *Mixed dissociated/molecular monolayer of water on the TiO_2(0 1 1)-(2 × 1) surface*, Surf. Sci. 591 (2005), pp. L267–L272.

[51] G. Ketteler, S. Yamamoto, H. Bluhm, K. Andersson, D.E. Starr, D.F. Ogletree, H. Ogasawara, A. Nilsson, and M. Salmeron, *The nature of water nucleation sites on TiO_2(110) surfaces revealed by ambient pressure X-ray photoelectron spectroscopy*, J. Phys. Chem. C 111 (2007), pp. 8278–8282.

[52] L. Giordano, J. Goniakowski, and J. Suzanne, *Partial dissociation of water molecules in the (3 × 2) water monolayer deposited on the MgO (100) surface*, Phys. Rev. Lett. 81 (1998), pp. 1271–1273.

[53] T. Hikita, T. Hanada, M. Kudo, and M. Kawai, *Surface-structure of $SrTiO_3$(001) with various surface treatments*, J. Vacuum Sci. Technol. A:Vacuum Surf. Films 11 (1993), pp. 2649–2654.

[54] N. Erdman, K.R. Poeppelmeier, M. Asta, O. Warschkow, D.E. Ellis, and L.D. Marks, *The structure and chemistry of the TiO_2-rich surface of $SrTiO_3$ (001)*, Nature 419 (2002), pp. 55–58.